Cavity Quantum Electrodynamics with Anderson-Localized Modes

Luca Sapienza *et al.*

Science **327**, 1352 (2010);
DOI: 10.1126/science.1185080

Science (print ISSN 0036-8075; online ISSN 1095-9203) is published weekly, except the last week in December, by the American Association for the Advancement of Science, 1200 New York Avenue NW, Washington, DC 20005.

References and Notes

1. D. H. Hathaway, *Astrophys. J.* **460**, 1027 (1996).
2. K. Topka, R. Moore, B. J. LaBonte, R. Howard, *Sol. Phys.* **79**, 231 (1982).
3. E. Ribes, P. Mein, A. Mangeney, *Nature* **318**, 170 (1985).
4. M. A. Kambry, J. Nishikawa, T. Sakurai, K. Ichimoto, E. Hiei, *Sol. Phys.* **132**, 41 (1991).
5. R. W. Komm, R. F. Howard, J. W. Harvey, *Sol. Phys.* **147**, 207 (1993).
6. C. R. DeVore, N. R. Sheeley Jr., *Sol. Phys.* **108**, 47 (1987).
7. A. A. van Ballegooijen, N. P. Cartledge, E. R. Priest, *Astrophys. J.* **501**, 866 (1998).
8. C. J. Schrijver, A. M. Title, *Astrophys. J.* **551**, 1099 (2001).
9. Y.-M. Wang, J. L. Lean, N. R. Sheeley Jr., *Astrophys. J.* **625**, 522 (2005).
10. J. L. Lean, D. H. Rind, *Geophys. Res. Lett.* **35**, L18701 (2008).
11. M. Dikpati, G. de Toma, P. A. Gilman, *Geophys. Res. Lett.* **33**, L05102 (2006).
12. A. R. Choudhuri, P. Chatterjee, J. Jiang, *Phys. Rev. Lett.* **98**, 131103 (2007).
13. L. Svalgaard, E. W. Cliver, Y. Kamide, *Geophys. Res. Lett.* **32**, L01104 (2005).
14. P. H. Scherrer *et al.*, *Sol. Phys.* **162**, 129 (1995).
15. N. R. Sheeley Jr., *Sol. Phys.* **9**, 347 (1969).
16. MDI Calibration Notes and Known Problems, http://soi.stanford.edu/data/cal
17. D. H. Hathaway, R. M. Wilson, *Sol. Phys.* **224**, 5 (2004).
18. J. G. Beck, P. Giles, *Astrophys. J.* **621**, L153 (2005).
19. P. M. Giles, T. L. Duvall Jr., P. H. Scherrer, R. S. Bogart, *Nature* **390**, 52 (1997).
20. J. Schou, R. S. Bogart, *Astrophys. J.* **504**, L131 (1998).
21. I. González Hernández *et al.*, *Astrophys. J.* **638**, 576 (2006).
22. C. J. Schrijver, Y. Liu, *Sol. Phys.* **252**, 19 (2008).
23. Y.-M. Wang, E. Robbrecht, N. R. Sheeley Jr., *Astrophys. J.* **707**, 1372 (2009).

24. The SOHO/MDI project is supported by NASA grant NAG5-10483 to Stanford University. SOHO is a project of international cooperation between ESA and NASA. L.R. was supported as a summer intern at NASA/Marshall Space Flight Center through the Marshall Space Grant Research Internship Project.

15 September 2009; accepted 13 January 2010
10.1126/science.1181990

Cavity Quantum Electrodynamics with Anderson-Localized Modes

Luca Sapienza,* Henri Thyrrestrup, Søren Stobbe, Pedro David Garcia, Stephan Smolka, Peter Lodahl*

A major challenge in quantum optics and quantum information technology is to enhance the interaction between single photons and single quantum emitters. This requires highly engineered optical cavities that are inherently sensitive to fabrication imperfections. We have demonstrated a fundamentally different approach in which disorder is used as a resource rather than a nuisance. We generated strongly confined Anderson-localized cavity modes by deliberately adding disorder to photonic crystal waveguides. The emission rate of a semiconductor quantum dot embedded in the waveguide was enhanced by a factor of 15 on resonance with the Anderson-localized mode, and 94% of the emitted single photons coupled to the mode. Disordered photonic media thus provide an efficient platform for quantum electrodynamics, offering an approach to inherently disorder-robust quantum information devices.

The interaction between a single photon and a single quantized emitter is the core of cavity quantum electrodynamics (QED) and constitutes a node in a quantum information network (*1*, *2*). So far, cavity QED experiments have been realized with a wide range of two-level systems, including atoms (*3*), ions (*4*), Cooper-pair boxes (*5*), and semiconductor quantum dots (*6*–*8*) coupled to photons confined in a cavity. A common requirement for all these implementations is highly engineered cavities, in some cases requiring nanometer-scale accuracy (*9*). Surprisingly, multiple scattering of photons in disordered dielectric structures offers an alternative route to light confinement. If the scattering is very pronounced, Anderson-localized modes form spontaneously. Anderson localization (*10*) is a multiple-scattering wave phenomenon that has been observed for, e.g., light (*11*), acoustic waves (*12*), and atomic Bose-Einstein condensates (*13*). We have demonstrated cavity QED with Anderson-localized modes by efficiently coupling a single quantum dot (QD) to a disorder-induced cavity mode (*14*) in a photonic crystal waveguide.

DTU Fotonik, Department of Photonics Engineering, Technical University of Denmark, Ørsteds Plads 343, DK-2800 Kgs. Lyngby, Denmark.

*To whom correspondence should be addressed. E-mail: lucs@fotonik.dtu.dk (L.S.); pelo@fotonik.dtu.dk (P.L.)

Photonic crystals are composite nanostructures in which a periodic modulation of the refractive index forms a photonic band gap of frequencies where light propagation is fully suppressed. By deliberately introducing a missing row of holes in a two-dimensional photonic crystal membrane, the periodicity is broken locally and light is guided (Fig. 1A). Such photonic crystal waveguides are strongly dispersive, i.e., light propagation depends sensitively on the optical frequency and can be slowed down. Engineering the photonic crystal waveguide enables the enhancement of light-matter interaction, which is required for high-efficiency single-photon sources (*15*) for quantum information technology (*1*, *16*). In the slow-light regime of photonic crystal waveguides, light propagation is very sensitive to unavoidable structural imperfections (*17*, *18*) and multiple-scattering events randomize propagation (*19*). Although multiple scattering is commonly considered a nuisance for a device, leading to optical losses, here the influence of wave interference in multiple scattering stops light propagation and forms strongly confined Anderson-localized modes (*10*) (Fig. 1B). Anderson-localized modes in a photonic crystal waveguide appear as a result of the primarily one-dimensional nature of the propagation of light provided that the localization length is shorter than the length of the waveguide (*20*).

We deliberately created Anderson-localized modes by fabricating photonic crystal waveguides with a lithographically controlled amount of disorder (Fig. 1B). The hole positions in three rows above and below the waveguide were randomly perturbed with a standard deviation varying between 0 and 6% of the lattice parameter. We investigated the Anderson-localized modes by recording QD photoluminescence spectra under high-excitation power where the feeding from multiple QDs makes Anderson-localized modes appear as sharp spectral resonances (Fig. 1C). The observation of spectrally separated random resonances is a signature of Anderson localization of light (*14*), while the detailed statistics of the intensity fluctuations unambiguously verifies localization even in the presence of absorption (*21*). Figure 1D shows the intensity distribution from spectra recorded at different spatial and spectral positions, which allow us to average over different realizations of disorder. Clear deviations from the Rayleigh distribution predicted for non-localized waves are observed. Light is localized if the variance of the normalized intensity fluctuations exceeds the critical value of 7/3 (*21*), and we extract a variance of 5.3, which proves Anderson localization.

Examples of Anderson-localized modes are shown in Fig. 2 as peaks appearing at random spectral positions, although limited to the slow-light regime of the photonic crystal waveguide. The latter property is due to the strongly dispersive behavior of the localization length that is considerably shortened in the slow-light regime. We tuned the spectral range of Anderson-localized modes by controlling the amount of disorder. Even in samples without engineered disorder, intrinsic and thus unavoidable imperfections, such as surface roughness, are sufficient to localize light (*22*).

The important cavity figures-of-merit are the mode volume V and the Q factor. Decreasing V leads to an enhancement of the electromagnetic field and thus improves light-matter coupling. The Q factor is proportional to the cavity storage time of a photon that needs to be increased for cavity QED applications. High Q factors ranging between 3000 and 10,000 are obtained for different degrees of disorder (Fig. 2) and are comparable to state-of-the-art values obtained for traditional photonic crystal nanocavities containing QDs (*7*).

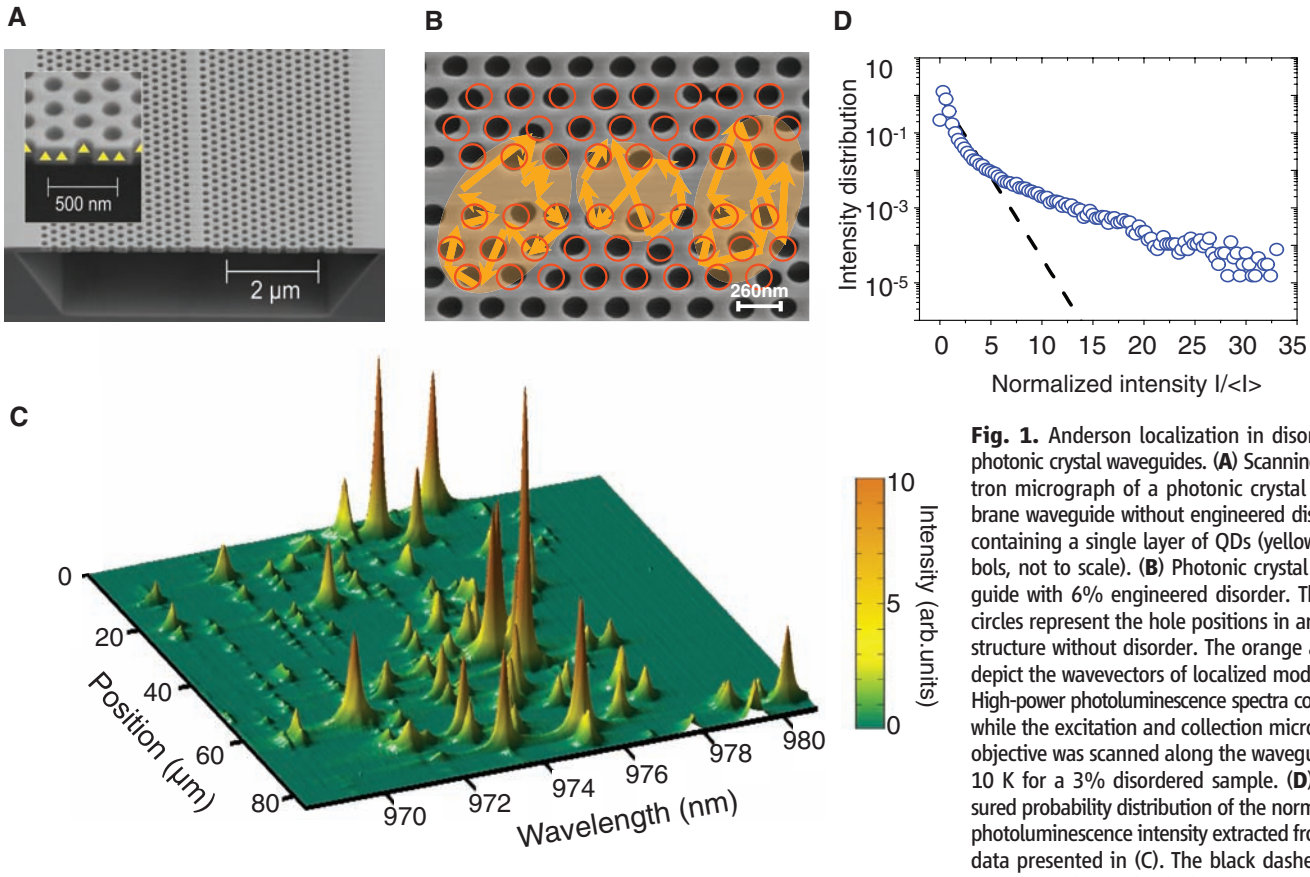

Fig. 1. Anderson localization in disordered photonic crystal waveguides. (**A**) Scanning electron micrograph of a photonic crystal membrane waveguide without engineered disorder, containing a single layer of QDs (yellow symbols, not to scale). (**B**) Photonic crystal waveguide with 6% engineered disorder. The red circles represent the hole positions in an ideal structure without disorder. The orange arrows depict the wavevectors of localized modes. (**C**) High-power photoluminescence spectra collected while the excitation and collection microscope objective was scanned along the waveguide at 10 K for a 3% disordered sample. (**D**) Measured probability distribution of the normalized photoluminescence intensity extracted from the data presented in (C). The black dashed line represents the Rayleigh distribution.

Anderson-localized cavities thus offer a fundamentally new route to cavity QED that is inherently robust to fabrication imperfections, as opposed to traditional cavities (*9*).

Pumping the sample at low-excitation power allowed us to resolve single QD lines and therefore to enter the regime of cavity QED. Figure 3A shows an example of a photoluminescence spectrum displaying single QD peaks and Anderson-localized cavities. QDs and cavity peaks can be easily distinguished from their different temperature dependences (Fig. 3B) that also enable the spectral tuning of single QDs into resonance with an Anderson-localized cavity. Figure 3C displays the crossing between a QD and an Anderson-localized cavity, demonstrating that the cavity-QD system is in the Purcell regime where the cavity promotion of vacuum fluctuations enhances the QD decay rate (*6*).

The Purcell enhancement is studied by means of time-resolved photoluminescence spectroscopy: A QD is repeatedly excited with a short optical pulse and the emission time is measured. Collecting many single-photon events allowed us to record a decay curve representing a histogram of detection events versus time. Two examples of decay curves for the QD tuned on- and off-resonance with an Anderson-localized cavity are presented in Fig. 4A. Off resonance, the QD decay rate is inhibited due to the two-dimensional photonic band gap, leading to an emission rate of 0.5 ns^{-1}. A pronounced enhancement by a factor of 15 is observed on resonance where a fast decay rate of 7.9 ns^{-1} is extracted. An important figure-of-merit for, e.g., single-photon sources or nanolasers is the β factor, which expresses the fraction of photons emitted into a cavity mode. By comparing the emission rates on and off resonance, we extract β = 94%, which represents a lower bound because even for large detuning, residual coupling to the waveguide can persist. The high β factor competes with results obtained on standard photonic crystal nanocavities with carefully optimized cavity design and QD density (*7*). Our results demonstrate that distributed photonic dis-

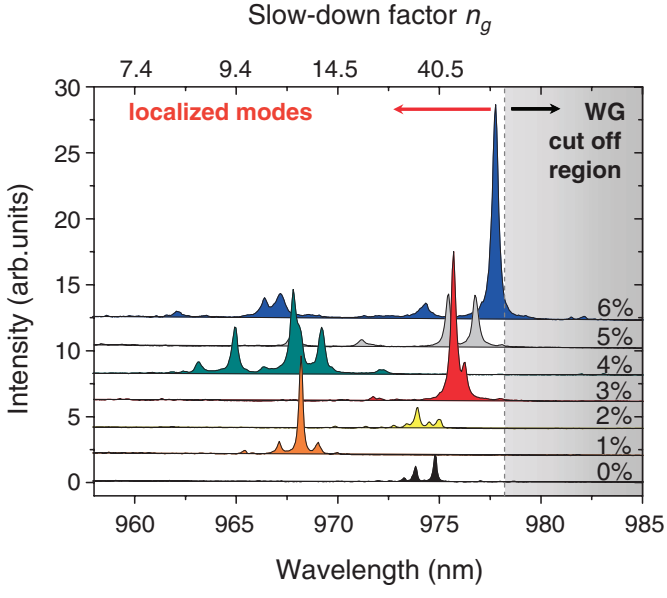

Fig. 2. Spectral signature of Anderson-localized modes. Photoluminescence spectra collected as in Fig. 1C, for various degrees of engineered disorder. Each spectrum was collected with the excitation and collection microscope objective at a fixed position on the waveguide and was vertically shifted for visual clarity. The gray area highlights the calculated waveguide (WG) cut-off region, assuming a refractive index of GaAs of 3.44. $n_g = \frac{c}{\partial\omega/\partial k}$ is the calculated group velocity slow-down factor for an ideal structure without disorder, where c is the vacuum light speed, ω is the frequency, and k is the wave number.

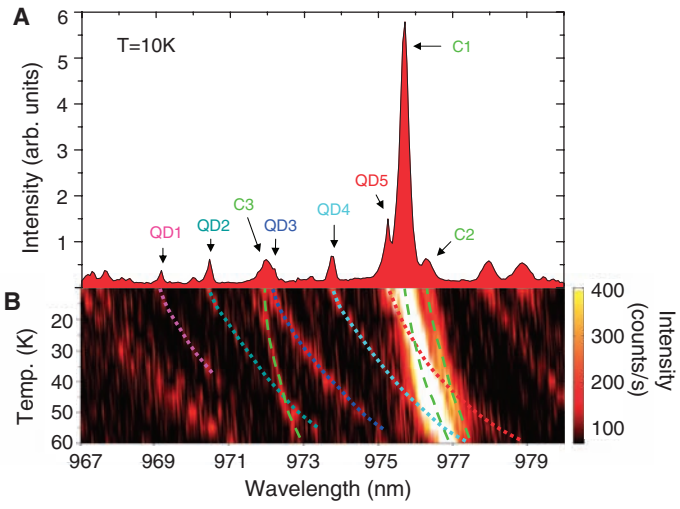

Fig. 3. Temperature tuning of single QDs into resonance with Anderson-localized cavities. (**A**) Low-power photoluminescence spectrum of a sample with 3% disorder at 10 K. (**B**) Photoluminescence spectra collected while varying the sample temperature in steps of 5 K. The dotted (dashed) lines are guides to the eye of the wavelength displacement of selected QD emission lines (localized modes). (**C**) Enlargement of the spectra displaying the QD-cavity crossing. The spectra are fitted to two Lorentzians (solid lines) representing the QD and the cavity peak.

order provides a powerful way of enhancing the interaction between light and matter, enabling cavity QED.

The decay rates of two individual QDs tuned across an Anderson-localized cavity are plotted in Fig. 4B. Different enhancement factors (15 and 9 at temperature T = 25 and 55 K, respectively) are observed on resonance due to the different positions and dipole orientations of the QDs that influence their coupling to the cavity mode. The presence of an additional Anderson-localized cavity gives rise to the asymmetric detuning dependence of the decay rate. Assuming a perfect spatial match between the QD and the cavity mode, we can extract an upper bound on the mode volume of the Anderson-localized cavity of $V \sim 1\ \mu m^3$ from the observed rate on resonance. By estimating the extension of the localized modes in the two directions orthogonal to the waveguide (*23*), we derive a cavity length of 25 μm for cavity C1. Establishing the fundamental lower limit of the cavity length relates to the fundamental question of determining the localization length of Anderson-localized modes. It is predicted that the localization length can be reduced below the wavelength of light, and it was even suggested that no fundamental lower boundary exists (*24*). Consequently, engineered disorder might pave a way to subwavelength confinement of light in dielectric structures.

Figure 4B shows that Purcell enhancement is observed mainly within the cavity linewidth, which is opposed to the surprisingly far-reaching coupling reported for standard photonic crystal cavities under nonresonant excitation (*7*). Consequently, the extracted QD decay rates are sensitive probes of the local photonic environment of disordered photonic crystal waveguides. Photon emission in disordered photonic structures was predicted to lead to a new class of infinite-range correlations manifested as fluctuations in the decay rate of embedded emitters (*25*). Thus, the Purcell enhancement stems from the local enhancement of the photonic density of states in the Anderson-localized regime that promotes spontaneous emission of photons.

QDs detuned from Anderson-localized cavities may couple to the slowly propagating mode of the photonic crystal waveguide. In this case, the QD decay rate is expected to scale proportional to the group velocity slow-down factor n_g (*26*). This behavior is observed for three different QDs at large detunings Δ from the dominating Anderson-localized cavity mode (Fig. 4C), i.e., here the radiative coupling is well described by the local photonic density of states of the unperturbed photonic crystal waveguide. This interesting coexistence of ordered and disordered properties occurs because relatively few periods of the photonic crystal lattice are required to build up the local environment determining the QD decay rate. Thus, the length scale on which the local photonic density of states builds up is mostly shorter than the localization length, which accounts for the success of photonic crystals despite ubiquitous disorder for, e.g., nanocavities (*9*), single-photon sources (*15*), or spontaneous emission control (*27*).

Our experiments demonstrate that disorder is an efficient resource for confining light in nanophotonic structures, thereby opening a new avenue to all-solid-state cavity QED that exploits disorder as a resource rather than a nuisance. Exploring disorder to enhance light-matter interaction and establishing the ultimate boundaries for this new technology provide exciting research challenges for the future, of relevance to not only QED but also other research fields that rely on enhanced light-matter interaction, such as energy harvesting or biosensing (*28*). Coupling several cavities is a potential way of scaling cavity QED for quantum information technology and represents one of the major challenges for engineered nanocavities. Controlled disorder might offer an interesting route to coherently couple cavities using so-called necklace states that are naturally occurring coupled Anderson-localized modes (*29*, *30*).

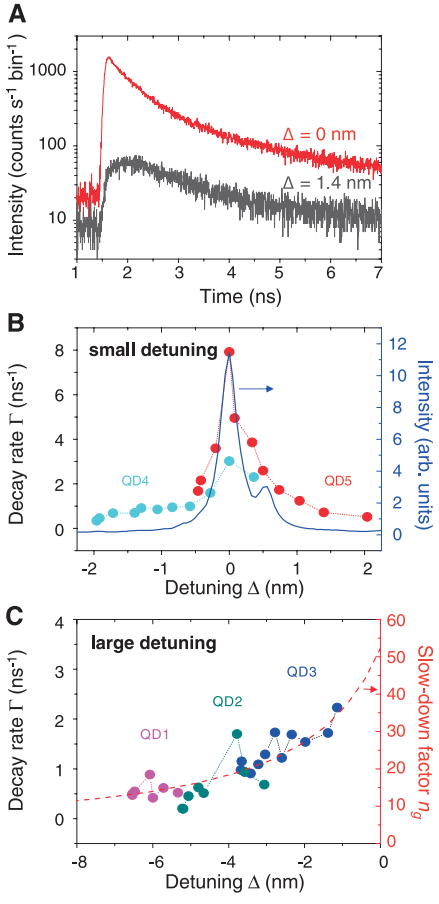

Fig. 4. Detuning dependence of single QD decay rates. (**A**) Decay curves of QD5 for two values of detuning Δ relative to the localized mode C1. (**B**) Decay rates of QD4 and QD5 versus detuning and cavity emission spectrum. (**C**) Decay rates of QD1, QD2, QD3 versus detuning. The dashed line is the calculated slow-down factor for the unperturbed photonic crystal waveguide. The enhancement at Δ = −4 nm stems from the coupling of QD2 to a weak Anderson-localized cavity mode (C3 in Fig. 3A).

References and Notes

1. H. J. Kimble, *Nature* **453**, 1023 (2008).
2. T. Wilk, S. C. Webster, A. Kuhn, G. Rempe, *Science* **317**, 488 (2007).
3. J. M. Raimond, M. Brune, S. Haroche, *Rev. Mod. Phys.* **73**, 565 (2001).
4. H. Häffner, C. F. Roosa, R. Blatt, *Phys. Rep.* **469**, 155 (2008).
5. A. Wallraff *et al.*, *Nature* **431**, 162 (2004).
6. J. M. Gérard *et al.*, *Phys. Rev. Lett.* **81**, 1110 (1998).
7. K. Hennessy *et al.*, *Nature* **445**, 896 (2007).
8. I. Fushman *et al.*, *Science* **320**, 769 (2008).
9. Y. Akahane, T. Asano, B.-S. Song, S. Noda, *Nature* **425**, 944 (2003).
10. P. W. Anderson, *Phys. Rev.* **109**, 1492 (1958).
11. D. S. Wiersma, P. Bartolini, A. Lagendijk, R. Righini, *Nature* **390**, 671 (1997).
12. H. Hu, A. Strybulevych, J. H. Page, S. E. Skipetrov, B. A. van Tiggelen, *Nat. Phys.* **4**, 945 (2008).
13. J. Billy *et al.*, *Nature* **453**, 891 (2008).
14. J. Topolancik, B. Ilic, F. Vollmer, *Phys. Rev. Lett.* **99**, 253901 (2007).
15. T. Lund-Hansen *et al.*, *Phys. Rev. Lett.* **101**, 113903 (2008).
16. E. Knill, R. Laflamme, G. J. Milburn, *Nature* **409**, 46 (2001).
17. S. Hughes, L. Ramunno, J. F. Young, J. E. Sipe, *Phys. Rev. Lett.* **94**, 033903 (2005).
18. S. John, *Phys. Rev. Lett.* **58**, 2486 (1987).
19. A. F. Koenderink, A. Lagendijk, W. L. Vos, *Phys. Rev. B* **72**, 153102 (2005).
20. S. Mazoyer, J. P. Hugonin, P. Lalanne, *Phys. Rev. Lett.* **103**, 063903 (2009).
21. A. A. Chabanov, M. Stoytchev, A. Z. Genack, *Nature* **404**, 850 (2000).
22. J. Topolancik, F. Vollmer, B. Ilic, *Appl. Phys. Lett.* **91**, 201102 (2007).
23. Materials and methods are available as supporting material on *Science* Online.
24. A. Lagendijk, B. van Tiggelen, D. S. Wiersma, *Phys. Today* **62**, 24 (2009).
25. B. Shapiro, *Phys. Rev. Lett.* **83**, 4733 (1999).
26. V. S. C. Manga Rao, S. Hughes, *Phys. Rev. B* **75**, 205437 (2007).
27. P. Lodahl *et al.*, *Nature* **430**, 654 (2004).
28. R. C. Somers, M. G. Bawendi, D. G. Nocera, *Chem. Soc. Rev.* **36**, 579 (2007).
29. J. B. Pendry, *J. Phys. C* **20**, 733 (1987).
30. J. Bertolotti, S. Gottardo, D. S. Wiersma, M. Ghulinyan, L. Pavesi, *Phys. Rev. Lett.* **94**, 113903 (2005).

31. We gratefully acknowledge T. Schlereth and S. Höfling for quantum dot growth, J.M. Hvam for discussions, and the Council for Independent Research (Technology and Production Sciences and Natural Sciences) and the Villum Kann Rasmussen Foundation for financial support.

Supporting Online Material

www.sciencemag.org/cgi/content/full/327/5971/1352/DC1
Materials and Methods
References

24 November 2009; accepted 20 January 2010
10.1126/science.1185080

Light-Controlled Self-Assembly of Semiconductor Nanoparticles into Twisted Ribbons

Sudhanshu Srivastava,[1] Aaron Santos,[1] Kevin Critchley,[1,2] Ki-Sub Kim,[1,3] Paul Podsiadlo,[1,4] Kai Sun,[5] Jaebeom Lee,[1,7] Chuanlai Xu,[1,8] G. Daniel Lilly,[1] Sharon C. Glotzer,[1,6]* Nicholas A. Kotov[1,5,6,7]*

The collective properties of nanoparticles manifest in their ability to self-organize into complex microscale structures. Slow oxidation of tellurium ions in cadmium telluride (CdTe) nanoparticles results in the assembly of 1- to 4-micrometer-long flat ribbons made of several layers of individual cadmium sulfide (CdS)/CdTe nanocrystals. Twisting of the ribbons with an equal distribution of left and right helices was induced by illumination with visible light. The pitch lengths (250 to 1500 nanometers) varied with illumination dose, and the twisting was associated with the relief of mechanical shear stress in assembled ribbons caused by photooxidation of CdS. Unusual shapes of multiparticle assemblies, such as ellipsoidal clouds, dog-bone agglomerates, and ribbon bunches, were observed as intermediate stages. Computer simulations revealed that the balance between attraction and electrostatic repulsion determines the resulting geometry and dimensionality of the nanoparticle assemblies.

Spirals, helicoids, helices, twisted ribbons (TRs), and other helical structures present fascinating geometries from the perspectives of mathematics, biology, optics, and mechanics. The formation of helices from nanoparticles (NPs) will make possible exploitation of the unusual properties of helices arising from quantum confinement (*1*, *2*) within NPs, as well as expand the design space (*3*, *4*) and offer new means of controlling the pitch and/or chirality of the helical structures. To achieve self-organization of such intricate objects, it is necessary to fine-tune the overall balance of forces, including anisotropy of interactions that drive assembly of NPs into larger structures. Control of these processes will require the discovery of many-body interactions at the nanoscale, as well as understanding their dynamics and capabilities of formation of complex self-organized patterns transitioning from nano- to microscale.

As a model system for realizing these goals, we used an aqueous dispersion of CdTe (*5*) NPs (emission maximum at 550 nm) prepared (*6*) with thioglycolic acid (TGA) as a stabilizer with the TGA-to-Cd^{2+} ratio close to 1.0, rather than the traditional value of 2.4 (*7*). Based on the variety of existing data (*1*, *6*, *8*), these NPs exhibit strong anisotropy due to permanent dipoles on them (*1*, *8*). The strongly reduced concentration of TGA is expected to lead to the elimination of tetrahedral apices, where the local concentration of TGA is the highest, and an increase of the average value of dipole on NPs. It also increases chemical reactivity of the NPs, which intricately interplays with the interparticle forces. After preparation, the CdTe NPs are precipitated by addition of methanol and centrifuged for 20 min, followed by redispersion in deionized water at pH = 9 (adjusted by addition of NaOH). The orange color of the NP solution turns dark green within ~72 hours, indicating that NP self-assembly has occurred.

TRs with distinctive helicity (Fig. 1, A, B, and D to F), were the primary product of the aging process (Fig. 1) (*6*). The length of the TRs made from CdTe typically ranged from 0.8 to 2 μm, but can be as long as 8 μm (Fig. 1). Some straight nanowires (NWs) were also produced as a secondary product (Fig. 1C) and were identified as well-studied single crystalline Te wires (fig. S1) (*7*). Unlike these NWs or other NP assemblies (*6*), the TRs were made from individual NPs layered on top of each other (Fig. 1, G to I). Their thickness, as determined by atomic force microscopy (AFM), was 10 to 12 nm and corresponds to three to four NP layers. The pitch of the CdTe TRs averaged ~350 nm (Fig. 1, E and F). The distribution between right- and left-handed twisting was approximately equal: 52% right and 48% left, which indicates a nearly racemic mixture of chiral isomers (fig. S2) (*7*). Remarkably, the helical ribbons form bundles in which all TRs have the same chirality. Instead of the typical red shift of optical features found in previous studies of NP assemblies (*6*, *9*, *10*), a gradual blue shift of the luminescence and absorption peaks was observed during formation of TRs (Fig. 2A). This observation normally would have indicated the decrease in delocalization volume of excitons in CdTe and, hence, a wholly different process is taking place than that previously reported. This phenomenon is rather unusual but can be understood when the entire process of transformation of NPs to helicoidal structures is discussed.

We first characterized the composition of the products with x-ray energy dispersive spectroscopy (XEDS). The atomic percent Cd:Te:S ratio for TRs and original CdTe NPs was 46:10:44 and 43:38:19, respectively. The assembly process is associated with considerable loss of Te and transition to CdS/CdTe NPs, in which the CdS phase is strongly dominant. This substantial change of

[1]Department of Chemical Engineering, University of Michigan, Ann Arbor, MI 48109, USA. [2]School of Physics and Astronomy, University of Leeds, Leeds LS2 9JT, UK. [3]Department of Chemical and Biological Engineering, Chungju National University, 72 Daehak-ro, Chungju, Chungbuk 380-702, Republic of Korea. [4]Center for Nanoscale Materials, Argonne National Laboratory, Argonne, IL 60439, USA. [5]Department of Materials Science and Engineering, University of Michigan, Ann Arbor, MI 48109, USA. [6]Department of Biomedical Engineering, University of Michigan, Ann Arbor, MI 48109, USA. [7]Department of Nanomedical Engineering, College of Nanoscience and Nanoengineering, Pusan National University, Miryang 627-706, Republic of Korea. [8]School of Food Science and Technology, Jiangnan University, Wuxi, Jiangsu 214122, China.

*To whom correspondence should be addressed. E-mail: sglotzer@umich.edu (S.C.G.); kotov@umich.edu (N.A.K.)